Interplay between ferromagnetism, SDW order, and underscreened Kondo lattice in UCu_2Si_2

R. Troć,[1,*] M. Samsel-Czekała,[1] J. Stępień-Damm,[1] and B. Coqblin[2]

[1]*Institute of Low Temperature and Structure Research, Polish Academy of Sciences, P.O. Box 1410, 50-950 Wrocław 2, Poland*

[2]*Laboratoire de Physique des Solides, CNRS-Université Paris-Sud, 91405 Orsay, France*

(Received 7 May 2012; published 27 June 2012)

Electrical resistivity and low temperature magnetoresistivity (MR) measurements made on a single crystal of UCu_2Si_2 are reported. By using as a phonon reference the temperature dependence of the electrical resistivity of $ThCu_2Si_2$, we could establish that UCu_2Si_2 has both ferromagnetic (FM) and Kondo behaviors, which can be described by the underscreened Kondo lattice model. Our MR measurements revealed the presence of magnetic fluctuations within the FM order as it had been reported before for UGe_2. Also, one of the calculated Fermi surface sheets exhibited nesting properties, being in perfect agreement with the previous neutron diffraction data, which supports the possibility of the presence of the spin-density wave (SDW) phase. In the ternary silicide considered here in the region of temperatures where the strong FM order exists, this phase is signalized by magnetic fluctuations. The latter may emerge as an ordered antiferromagnetic (AFM) phase of an SDW-like character when the local ferromagnetism disappears at a slightly lower temperature than its T_N. The differences in the lack or observation of these two transitions in the temperature run were found to be strongly sample dependent.

DOI: 10.1103/PhysRevB.85.224434 PACS number(s): 73.43.Qt, 75.30.Mb, 75.30.Fv, 71.18.+y

I. INTRODUCTION

We present the physical properties of the UCu_2Si_2 compound, which was reported to be a ferromagnet with the Curie temperature $T_C = 103(3)$ K such as UCu_2Ge_2 ($T_C = 107$ K).[1] The other members of the $UT_2(Si;Ge)_2$ family (T = transition metal), also crystallizing in the most wide-spread body-centered tetragonal $ThCr_2Si_2$-type structure (space group $I4/mmm$)[2] as the previous two Cu-based ternaries, are either Pauli paramagnets or antiferromagnets.[3] Among this family of compounds, there is also the URu_2Si_2 compound with its hidden order,[4] which has been recently studied within the underscreened Anderson lattice (UAL) model,[5] as well as the ferromagnetic (FM) uranium silicides and germanides with Mn, both with T_C being slightly above room temperature (RT), but apart from the U $5f$ electrons the Mn $3d$ electrons also carry here a magnetic moment.[6]

As shown by neutron diffraction experiments made on powder[1,7] and single-crystalline[8] samples, the Cu-based silicide has a complex magnetic behavior at low temperatures with the ordered moment of 1.61(5) μ_B[1] or even 2.0 (1) μ_B,[7,8] oriented along the [001] direction (c axis). As demonstrated earlier on the polycrystalline samples, some homogeneity region with respect to a Cu/Si site exchange was revealed.[9] Also the fairly large differences in the value of the FM moment μ_f of U atoms in UCu_2Si_2 are believed to arise from some deficiency of Cu atoms in this compound, while any excess in the Cu content leads to a narrowing of domain walls. The latter, in turn, gives rise to a strong magnetocrystalline anisotropy effect.[9] Moreover, earlier studies based on ac-susceptibility, χ_{ac}, measurements[10,11] of polycrystalline UCu_2Si_2 samples suggested also an antiferromagnetic (AFM) order corresponding to a very small maximum in χ_{ac} within a few degrees above T_C. Quite surprisingly, the first single-crystal study of UCu_2Si_2 obtained by the Cu-flux method has revealed, except for the aforementioned observations, an additional AFM ordering but below T_C with the Néel temperature $T_N = 50$ K.[12] In contrast to the latter result, more recent single crystal studies of this compound, now using crystals grown by the Sn-flux procedure,[13] have indicated that besides an FM state being stable in the whole temperature range below T_C (=100 K), there really exists an AFM order but only between T_C and T_N (=106 K). A detailed neutron single-crystalline examination of this phase[8] has recently revealed an incommensurate longitudinal spin-density wave state (IL-SDW) with a very long periodicity $\Lambda = 85.7$ Å and a sinusoidal magnetic modulation with a propagation vector $\mathbf{k_z} = [0, 0, \delta]$, where $\delta = 0.116$ at 101 K. The fundamental modulation amplitude of order 1.3 μ_B, for which the root-mean-square average is equal to 0.9 μ_B, is close to the FM moment near T_C of 0.8 μ_B. The δ value grows a little with increasing temperature. In consequence, the magnetic structure contains as many as 17 layers with the in-plane sinusoidally modulated FM order. On the other hand, another single-crystalline sample of UCu_2Si_2 obtained by the Cu-flux method,[14] such as that reported in Ref. 12, has shown no AFM phases either below or above T_C. The saturation of the magnetic moment was determined to be 1.55 μ_B, being rather a low value but close to that obtained by the powder neutron diffraction.[1] Also from a single-crystal magnetization probe on UCu_2Si_2, a somewhat higher saturation value of μ_f (=1.75 μ_B) was reported in Ref. 13.

In recent years, the electronic structure of uranium compounds has been extensively studied by several models, band calculations, a model describing the dual nature of the $5f$ electrons,[15] or more recently by an underscreened Kondo lattice (UKL)[16] model. In turn, the ternary compounds of the $UT_2(Si;Ge)_2$ family have been extensively investigated by means of self-consistent density functional theory (DFT) calculations.[17] These calculations were carried out within the fully relativistic augmented spherical wave (ASW) method, including the effects of spin polarization and spin-orbit (SO) interactions. A continuation of the work presented in Ref. 17 was made by including so-called orbital polarization (OP)

corrections,[18] and this approach leads to better agreement between the theory and experiment concerning the magnitude of the orbital moment.

The electronic structure of this series of compounds first of all can be characterized by the relative energy positions of the d states of a given T atom compared with those of the uranium $5f$ states. They determine mainly the strength of hybridization between these electrons. Only for both UCu_2Si_2 and UPd_2Si_2, the Td states lie considerably lower in energy than the U $5f$ states and are separated from the latter by an energy interval of about 4 and 2 eV, respectively.[17,19]

In the case of UCu_2Si_2, the $3d$ and $5f$ states are the most distant in energy from the Fermi level (E_F), and the f-d hybridization in this compound is, therefore, considered to be the smallest one among all this family of 1:2:2 silicides.[19] Hence, both the increased average binding energy (BE) of the Cu $3d$ band and the increased d-band filling imply a smaller hybridization and a possible localized character of the $5f$ electrons. Thus, it is clear that in this Cu-based silicide, the U $5f$ states are sufficiently localized to carry the local magnetic moment. In consequence, it brings about a significant Kondo-like effect due to its interaction with the conduction band. This FM behavior of UCu_2Si_2 is consistent with the recently derived theoretical UKL[16] or UAL[20] models, both mentioned above, which describe well the coexistence of the combined FM and Kondo interactions, without including and including a finite $5f$ bandwidth, respectively. Indeed, the situation of uranium compounds appears to be rather different from that of cerium systems. In the former compounds one expects a very different interplay between the Kondo effect and magnetism, which leads to a rather strong FM ordering occurring at more than one order of magnitude larger T_C than those in the latter systems. In addition, they also show a logarithmic Kondo-type decrease of the resistivity above T_C but leads only to a partially Kondo-screened ordered uranium moment. These theoretical models and their applications to UCu_2Si_2 have already been briefly discussed in a conference paper,[21] and they will be discussed in the last section.

On the other hand, from the band structure calculations, we learn that the highest density of states (DOS) at the Fermi level, $N(E_F)$, among all these ternary compounds is just that found in UCu_2Si_2. Finally, results of band structure calculations using different approaches, being discussed below, and compared to the x-ray photoemission results obtained in RT measurements of single-crystalline UCu_2Si_2 have very recently been presented in Ref. 22. Thus, based on these calculations, we display here the derived topology of the Fermi surface (FS) of UCu_2Si_2, which has allowed us to predict the IL-SDW phase mentioned above. At the same time, de Haas-van Alphen (dHvA) oscillations measured at 30 mK and in a magnetic field of 17 T on the Sn-flux single crystal have recently revealed several branches, which correspond to moderately large cyclotron effective masses ranging from 1.4 to 4.2 m_0.[23] Then, the multiply connected FS were also calculated by using the relativistic spin-polarized linearized augmented plane wave (RSPLAPW) method[24] and compared to the aforementioned experimental results, which finally are explained by the $5f$ band model. As to our comparative analysis of the FS topology, we only mention here that it is based on a different approach, which will be described in detail below.

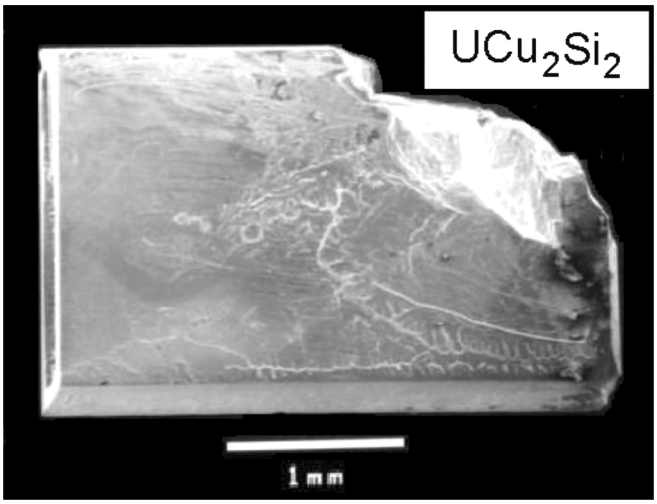

FIG. 1. One of the single crystals obtained by the Cu-flux method.

Continuing our previous magnetic bulk studies,[14] we present in this paper the electrical transport properties of single-crystalline UCu_2Si_2 derived in zero and in magnetic fields up to 8 T. Furthermore, the electrical measurements made on the reference compound $ThCu_2Si_2$ have allowed us to separate the phonon part from the total resistivity of uranium compound in the paramagnetic state. Thus, we will study here both the Kondo effect and the FM state in UCu_2Si_2 and discuss the observed coexistence between these two effects within the theoretical models mentioned above. We will give also a new explanation of an account of the occurrence of the IL-SDW phase after the disappearance of ferromagnetism at its T_C.

II. EXPERIMENTAL DETAILS

A single crystal of UCu_2Si_2 has been grown by the Cu-flux method described in Ref. 14. No further heat treatment of the sample was performed. The starting elements (with purity in weight percent) were U (99.98), Cu (99.99), and Si (99.999). Figure 1 shows one single crystal with a size $1.5 \times 1.5 \times 2.5$ mm^3 chosen from a number of similar ones. They were also in the form of thin platelets of different sizes. The largest flat surface of the single crystal visualized in Fig. 1 corresponds to the (001) plane. The specimens for an investigation of magnetic and electrical transport properties were cut from such a crystal using a wire saw. The purity and proper stoichiometric composition of the used single crystals were investigated by x-ray diffraction and an energy dispersive x-ray (EDX) analysis using a Phillips 515 scanning electron microscope equipped with a PV 9800 spectrometer.

A single-crystal x-ray refinement was performed at RT on an X-caliber 2 four-circle diffractometer equipped with a Charged-Coupled Device (CCD) camera using a graphite-monochromatized Mo Kα radiation. The intensities of reflections were corrected for Lorentz and polarization effects. The crystal data were refined by the full least-squares method using the SHELX-97 program.[25] In order to have nonmagnetic appropriate reference material, we synthesized a polycrystalline

sample of $ThCu_2Si_2$ by arc melting stoichiometric amounts of the elements (Th with purity 3N and the remaining elements, as mentioned above) under argon atmosphere. The obtained button was annealed under vacuum at 800 °C for about one week. The single phase feature was established by x-ray analysis using Cu Kα radiation. All the lines were indexed on a tetragonal $ThCu_2Si_2$-type unit cell (u.c.) as is the case of UCu_2Si_2. The u.c. parameters are in good agreement with the data published previously.[26,27] $ThCu_2Si_2$ was reported in earlier studies to be diamagnetic, which indicates its completely filled copper 3d shell and the lack of 5f electrons.[28]

In view of the former detailed susceptibility and magnetization investigations of a UCu_2Si_2 single crystal,[14] we have made here only a limited additional magnetic study. Thus, in order to probe the magnetic behavior, being controversial due to the presence of low and high temperature AFM phases in this silicide widely discussed in the literature (see, e.g., Kuznietz *et al.*[29,30]), we have made the low-frequency (1000 Hz) ac-magnetic susceptibility measurements at a small ac-field of 1 Oe as a function of temperature using a PPMS Quantum Designed apparatus. We have also performed magnetization measurements only at 4.2 K up to 5 T and in the temperature range 2–120 K at a magnetic field of 0.1 T using a commercial superconducting quantum interference device (SQUID) magnetometer. Electrical resistivity measurements were carried out using a steady-current four-point method with spot-welded wire contacts on bare-shaped specimens at temperatures between 4.2 and 300 K and in transverse magnetic fields ($\mathbf{j} \perp \mathbf{B}$) up to $B = \mu_0 H = 8$ T. The geometrical factor of the sample was determined with accuracy not lower than about 20%. The thermoelectric power (TEP) in the temperature range from 4.2 K to 300 K has been measured in a zero applied magnetic field. For electrical and TEP experiments, the specimens were cut out to the dimensions of about 2.5 × 1 × 1 mm^3 along the [001] and [100] directions of the crystal. During the latter measurements the temperature difference (ΔT) at the lowest temperatures was kept of the order 0.3 K along the sample while above 20 K, $\Delta T = 2$ K.

III. RESULTS AND DISCUSSION

A. Crystal structure

The single-crystalline refinement of the u.c. parameters is listed in Table I. The lattice parameters are in good agreement with the powder[1,9] and previous single-crystalline[12,13] data. Despite a small region of a homogeneity concentration existing in UCu_2Si_2,[9] the differences in lattice parameters vary quite negligibly. The refined free parameter z for the silicon atom at the 4e position (Table II) found here [$z = 0.3823(3)$] is comparable to those derived from the powder neutron diffraction experiment [0.3842(5)][1] and previous limited x-ray single crystal refinement [0.383(1)].[13] Moreover, the occupancy factors for all atomic positions of three kinds of constituent atoms have been established as 1.00(9). This value indicates that the studied single crystal is almost stoichiometric (see Table I). The anisotropic thermal displacement (ATD) factors (given only here) together with equivalent isotropic thermal displacement parameters $U_{(eq)}$ for the atoms in UCu_2Si_2 are also shown in Table II.

TABLE I. Crystal data and structure refinement for UCu_2Si_2.

Structure parameters RT data	
Empirical formula	Cu_2 Si_2 U
Formula weight	421.29
Temperature	293(2) K
Wavelength	0.071073 nm
Crystal system, space group tetragonal,	$I4/mmm$
Unit cell dimensions	$a = 0.3985(1)$ nm
	$c = 0.9945(2)$ nm
Volume	0.15793(6) nm^3
Z, Calculated density	2, 8.859 mg m^{-3}
Absorption coefficient	64.941 mm^{-1}
$F(000)$	356
θ range for data collection	4.10°−47.10°
Limiting indices	$-7 \leqslant h \leqslant 4$, $-8 \leqslant k \leqslant 7$, $-20 \leqslant l \leqslant 15$
Reflections collected/unique	1691/250 [R(int) = 0.1154]
Refinement method full-matrix least-squares on F^2	
Data/restraints/parameters	250/0/12
Goodness-of-fit on F^2	1.085
Final R indices [$I > 2\sigma(I)$]	$R_1 = 0.0437$, $wR_2 = 0.09255$
R indices (all data)	$R_1 = 0.0446$, $wR_2 = 0.0931$
Extinction coefficient	0.0021(19)
Largest diff. peak and hole	6114 and −6002 e. nm^{-3}

The coordination around uranium (as well as for thorium) is eightfold with silicon atoms at the corners of a flattened cube U(Th)Si_4 (D_{4h} point symmetry) with more ionic character between atoms (see Table III). At the same time, the $CuSi_4$ tetrahedra are strongly covalently bonded, as the results of crystal orbital overlap population (COOP) calculations, implemented within the ASW method, have shown.[31] These calculations have also predicted that the U–Cu bond plays rather a marginal role, so that all these considerations point to a large degree of localization of the 5f electrons with a weak hybridization with the 3d electrons in UCu_2Si_2, as reported in Ref. 19. On the other hand, all the previous considerations neglect, in fact, the p-f mixing mechanism,[32] which may markedly influence also the 5f-electron magnetism. Hence, Żołnierek and Mulak[33] have presented a description of the observed magnetic behavior of the whole group of the 1:2:2 uranium silicides and germanides in view of a competition between the single-ion crystal field and two-ion exchange

TABLE II. Atomic coordinates, anisotropic and equivalent isotropic displacement parameters (nm^2 × 10) for UCu_2Si_2. $U_{(eq)}$ is defined as one-third of the trace of the orthogonalized U_{ij} tensor. The anisotropic displacement-factor exponent takes the form $-2\pi^2[h^2a^{*2}U_{11} + \cdots + 2hka^*b^*U_{12}]$ and $U_{12} = U_{13} = U_{23} = 0$.

Atom	Site	x	y	z	$U_{(eq)}$	U_{11}	U_{22}	U_{33}
U	2a	0	0	0	11(1)	9(1)	9(1)	13(1)
Cu	4d	0	1/2	1/4	11(1)	10(1)	11(1)	13(1)
Si	4e	0	0	0.3823(3)	10(1)	9(1)	9(1)	13(1)

TABLE III. Selected interatomic distances (nm).

U−8 Si	0.3052(1)	Cu−4 Si	0.2388(2)
−8 Cu	0.31861(5)	−4 Cu	0.28178(7)
–2 Si	0.3802(3)		
−4 U	0.3985(1)		
−4 U	0.5636(1)		
		Si−Si	0.2341(7)
		−4 Cu	0.2388(2)
		−4 U	0.3052(1)

anisotropy. Otherwise, this approach means incorporating the classical crystal electric field (CEF) model with hybridization effects. On this basis these authors claimed the key role of the CEF effects in understanding the magnetism of all uranium 1:2:2 ternaries.

B. Magnetic properties

In our previous paper on the magnetic properties of UCu_2Si_2[14] we presented the detailed magnetic results obtained on the Cu-flux single crystals, and we discussed also the earlier single-crystalline magnetic results reported in Refs. 12 and 13. The main difference in magnetization (M) behavior between the Sn-flux derived results[13] and those obtained on the Cu-flux single crystals[12,14] is either a lack of the critical field B_{cr} in the $M(T)$ curve or its presence with a relatively large value (about 1 T), respectively. As shown in Fig. 1 of Ref. 14, this feature brings about an almost quadratic hysteresis loop in $M(B)$ behavior and the coercive field $B_C = \mu_0 H_C \approx 1$ T, derived along the c axis. In Fig. 2 we display the magnetization vs magnetic field, $M(B)$, measured up to 5 T and taken in the wide range of temperatures 1.9–80 K. As seen, the differential susceptibility, dM/dB, up to 80 K is almost independent of an applied field. Moreover, a quite different hysteresis loop for similarly obtained single crystals has also been presented in Fig. 2 of Ref. 12. In fact, the authors claimed that they magnetized their single crystal, being in an AFM ground state, i.e., below $T_N = 50$ K. The latter results mean that even a modest external magnetic field of an order of 1 T, applied parallel to the c axis at 5 K, were enough to start inducing the fully ordered FM state of $\approx$1.8 μ_B at slightly higher field strengths. In contrast to our results given in Ref. 14, the lack of symmetry in the hysteresis loop presented in Ref. 12 and some steplike change in the magnetization observed at $\mu_0 H_C \approx$ 2 T make this loop puzzling. In addition, this magnetization loop does not remind any classical metamagnetic transition as would be expected. Nevertheless, it simply looks like in the case of the latter type of single crystals obtained in the Cu-flux procedure owing to a huge anisotropy we have to do with narrow domain walls, which in turn leads to the intrinsic pinning of them in zero or in weaker applied magnetic fields. Earlier, McElfresh *et al.*[34] have shown, from the demagnetization measurements made from 5 T at 5 K on a polycrystalline sample, the existence of a high coercivity field, $\mu_0 H_C = 1.7$ T, which is well consistent with the effect of huge anisotropy. For the purpose of addressing this question, Roy *et al.*[35] also measured B_C but as a function of temperature on a similar kind of a sample. They showed a dramatic increase in B_C below about 70 K, which indicates the important role of a strongly temperature-dependent anisotropy in this system observed mainly at low temperatures. Our previous magnetization results[14] and those presented in Fig. 2 confirm entirely the previous conclusions.

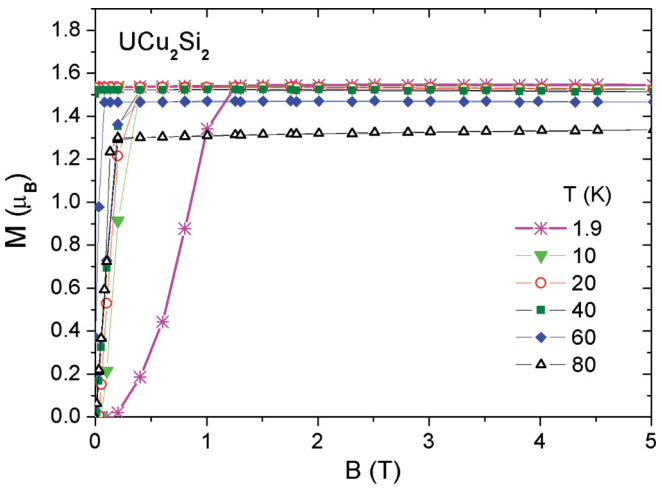

FIG. 2. (Color online) Magnetization taken in the temperature range 1.9–80 K against magnetic fields up to 5 T.

Furthermore, in Fig. 3(a) the temperature-dependent ac-susceptibility measurements with the in-phase χ' and out-of-phase χ'' components, made for the first time on the single-crystalline sample of UCu_2Si_2, are displayed. For comparison, we have plotted in this figure also the only available complete $\chi_{ac}(T)$ curves, reported in Ref. 11, for the polycrystalline sample. As one can see from this figure, both sets of peaked curves exhibit a large similarity in their form except for their wide spreading temperature. As seen, the single-crystalline curves are much narrower. Moreover, instead of the small feature marked as T_N^* [being apparent in both $\chi_{ac}(T)$ curves],[10,11] we found the only shallow curvature marked as T_N. This gives evidence that the difference between T_C and T_N in the case of our single-crystalline sample, if it really exists, is very small in relation to that (5–7 K) reported by other authors. It should be also mentioned that the small features in $\chi_{dc}(T)$ were also observed on both kinds of samples, poly- and single-crystalline ones.[10,13,34] Furthermore, in Fig. 3(b) we present the magnetization curve $M(T)$ taken on a set of pure thin single-crystalline platelets oriented along the easy magnetization direction by an applied magnetic field of 0.1 T. Next, in the inset of this figure, we display the temperature derivative of the magnetization, $dM(T)/dT$, which also presents a shallow anomaly at T_N with a similar difference to T_C, as we mentioned above. Despite these weak shallow anomalies observed in our ac-susceptibility and low field magnetization experiments, we were not able to detect any metamagnetic transition in our $M(B)$ curves taken in the temperature range 98–120 K (Fig. 3 in Ref. 14). Moreover, we found only one sharp maximum in our specific heat data at $T_C = 103$ K.[36] It is worthwhile emphasizing here that the authors of both single-crystalline specific heat measurements[12,13] did observe exactly the two transitions at T_C and T_N^*.

These observed distinct differences between our study and the other studies made on the single-crystalline samples

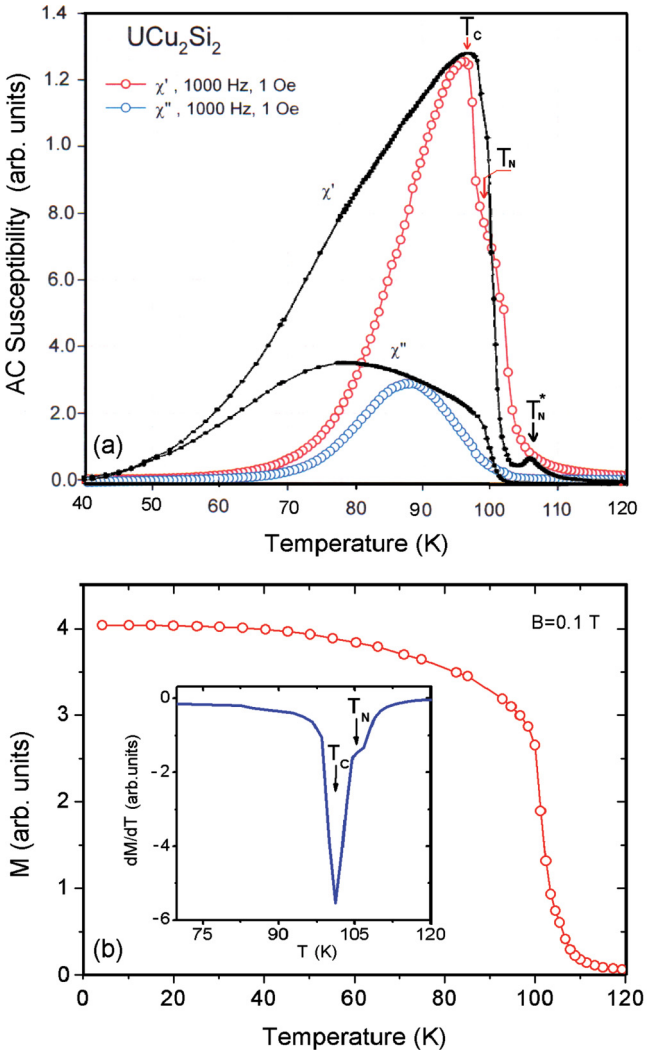

FIG. 3. (Color online) (a) Ac-susceptibility curves (measured along the easy magnetization axis c) vs temperature for two cases: powder data from Ref. 11 (black curves) and single-crystalline data of the present paper (open symbols). (b) Magnetization vs temperature taken at magnetic field of 0.1 T on a number of thin single-crystalline platelets. The inset shows the derivative dM/dT as a function of temperature.

will be discussed below. We should mention here also the differences occurring in a value of the uranium FM moment μ_f reported in various works, i.e., 1.55–1.61,[1,14] 1.75,[13] 1.8,[12] and 2.0 μ_B.[7,8] Hiebl *et al.*[9] investigated several polycrystalline samples synthesized with some deficiency or excess in the Cu atoms. They revealed that the maximum saturation moment value is increased even by 30% in the case of some deficiency of Cu in relation to the case of full stoichiometry. On the other hand, any excess in this element correlates with a strong magnetocrystalline anisotropy, indicating the presence in such a type of sample of narrow domain walls. Hence, it seems that the observed distinct changes in the previous magnetic parameters, as the transition temperatures or saturation moments, depend strongly on the mutual atomic ratio of the contents in the studied compound. All the previous objections may point to the fact that our single crystal has almost stoichiometric composition and that it differs in some degree from the other samples probed previously by different authors.

C. Electrical resistivity and magnetoresistivity

We present here our analysis of the experimental resistivity data. There are three parts in this discussion: the first part concerns the anisotropy of the resistivity due to the strongly anisotropic nature of UCu_2Si_2; the second part is the explanation of the FM-Kondo behavior by the UKL or UAL models;[16,20] and the third part is devoted to the magnetoresistivity (MR).

The electrical resistivity $\rho_i(T)$ of UCu_2Si_2 measured for the current $\mathbf{j}$ flowing along $i = a$ and c axes, is shown in Figs. 4(a) and 4(b), respectively. Note that different temperature scales were applied.

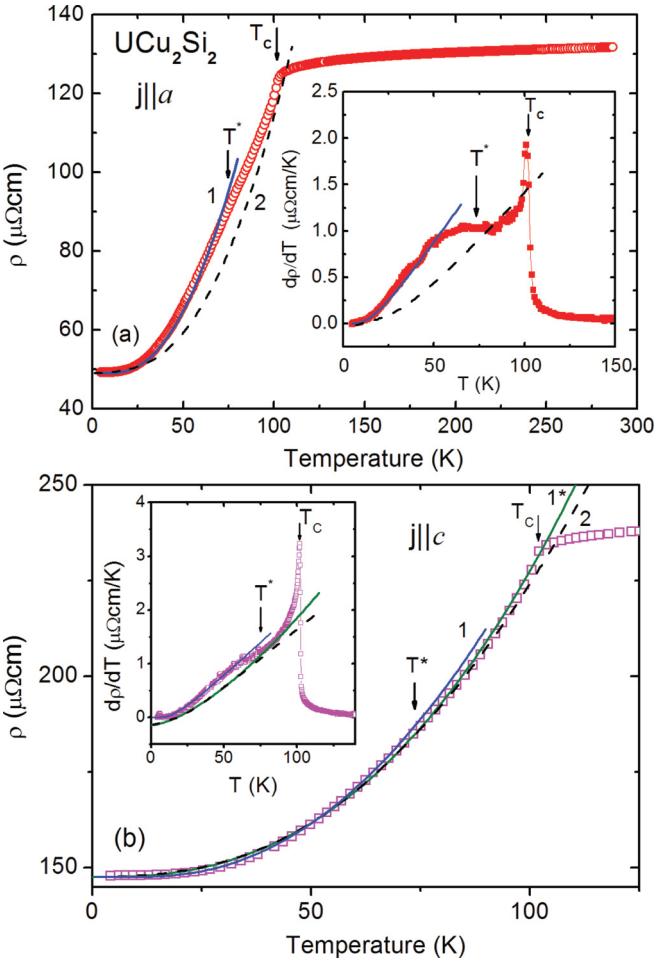

FIG. 4. (Color online) Electrical resistivity vs temperature for two current directions: (a) parallel to the a axis, and (b) parallel to the c axis. Curves (1) and (2) denote the fittings of Eqs. (1) and (2), respectively, to the experimental data with $n = 2$. Curve (1*) denotes the case $\mathbf{j}\|c$, in which Eq. (1) was used in the entire ordered region with $n = 2.5$. The insets present the corresponding temperature dependencies of the experimental temperature derivatives of the resistivity. The solid and dashed curves illustrate the temperature dependencies of the theoretical resistivity derivatives of functions described by Eqs. (1) and (2) with the parameters given in Tables IV(a) and IV(b), respectively.

TABLE IV. (a) Parameters of fitting by Eq. (1) for the curves [$C(j)$] displayed in Figs. 4(a)) and 4(b). (b) Parameters of fitting by Eq. (2) for the curves displayed in Fig. 4.

(a) Current	n	ρ_o ($\mu\Omega$ cm)	A_i ($\mu\Omega$ cm K^{-n})	Δ (K)
$\mathbf{j}\|a$ C(1)	2	49.0	0.0140	40
$\mathbf{j}\|c$ C(1)	2	147.5	0.0125	40
$\mathbf{j}\|c$ C(1*)	2.5	147.5	0.0008	0
(b) Current	ρ_o ($\mu\Omega$ cm)	A ($\mu\Omega$ cm K^{-2})	B ($\mu\Omega$ cm K^{-1})	Δ (K)
$\mathbf{j}\|a$ C (2)	49.0	0.0025	0.54	125
$\mathbf{j}\|c$ C (2)	147.5	0.0038	0.35	100

The results indicate a strong anisotropic behavior of the resistivity of this compound caused mainly by various and relatively large values of the residual resistivities ρ_{0i}, accounting 49 and 148 $\mu\Omega$ cm for $\mathbf{j}\|a$ and c, respectively. However, the magnitudes of the difference ($\rho_i - \rho_{0i}$) at RT are almost equal to each other for these two current directions. The resistivities ρ_a and ρ_c below RT only slightly decrease with decreasing temperature down to T_C. A similar situation exists, for example, in the isostructural UPd_2Si_2, although having AFM ordering at low temperatures.[37] Also the ratio ρ_{0c}/ρ_{0a} is about 3 for the Cu-based compound. In contrast to the above results, the study of Sn-flux UCu_2Si_2 single crystal indicates negligible values of ρ_{0i} as well as the lack of B_C in the magnetization curve along the easy c axis. The latter has already been treated in Sec. III B. These varying results of the two papers may point to the fact that we deal here with the strongly anisotropic ferromagnet, which may lead to large and anisotropic residual resistivities. As one can expect, near T_C there is a well-marked knee in $\rho_i(T)$ curves for both current directions. It is not, however, surprising that we do not observe here a small kink at T_N (=106 K), as that in Fig. 3 of Ref. 13, because in our case this temperature almost does not differ from T_C. Next, below this transition temperature, one observes a rapid decrease in $\rho_i(T)$ behavior due to a graduate vanishing of the spin-order resistivity contribution. This process proceeds, however, with some deviation from a monotonic dropping line, such as that observed in classical ferromagnets, but it shows some *bulge* in the intermediate region of temperatures. Therefore, we tried to fit first of all the low temperature dependence of the resistivity to the power curves using Eq. (1), because in the case of an anisotropic ferromagnet an energy gap Δ should be taken into account in its spin-wave energy spectrum,

$$\rho_i = \rho_{i0} + A_i T^n \exp(-\Delta/T). \quad (1)$$

As seen in Figs. 4(a) and 4(b), such fittings, marked as curve (1), follow the above equation with an index $n = 2$ and $\Delta = 40$ K for both current directions up to about 60 K [for the coefficient A_i, see Table IV(a)]. These results are in general agreement with the findings of other authors who have studied the polycrystalline samples of UCu_2Si_2.[11] We found also that if we omitted the experimental points in the intermediate range of temperatures where the bulge appears, we were able to consider, for example, $\rho_c(T)$ in the FM state, to get a fairly good fitting with $n = 2.5$ but with $\Delta = 0$ over the whole temperature range of the ordered state [see in Fig. 4(b) curve (1*)] with the A_c value given in Table IV(a).

It is interesting to note that a reasonable fit over the whole temperature range in the FM state (keeping, however, the previous temperature range limit of the bulge) could be also obtained when applying Eq. (2), being commonly used in a similar type of compounds,[38]

$$\rho(\mathrm{T}) = \rho_0 + \mathrm{AT}^2 + \mathrm{BT}(1 + 2\mathrm{T}/\Delta)\exp(-\Delta/\mathrm{T}). \quad (2)$$

Such a fitting curve, marked by number 2, is shown in Fig. 4(b) by a dashed line. This is probably also true in the case of $\rho_a(T)$, where the fitting is rather simulated due to a large contribution of extra electron scattering leading to the bulge. The best fit parameters describing Eq. (2) for both crystallographic directions are given in Table IV(b).

On the other hand, this bulge effect in $\rho_i(T)$ changes into a distinct *hump* in the temperature derivatives of the experimental resistivity $d\rho_i(T)/dT$, determined along both main axes, as shown in the insets of Figs. 4(a) and 4(b). In these insets, we also plotted the curves as being the derivatives of the corresponding Eqs. (1) and (2). This allows one to appreciate the magnitude of these experimental $d\rho_i(T)/dT$ humps as being much larger for $\mathbf{j}\|a$ than $\mathbf{j}\|c$, while the magnitudes of the sharp jumps of the above derivative at the corresponding T_C's is quite in a reverse relation.

The occurrence of the hump in the temperature derivative of the resistivity is probably connected with the crossover at T^*, thoroughly described in the case of UGe_2 (see, e.g., Ref. 39). A similar result was also found earlier for the polycrystalline sample of UCu_2Si_2 but without giving a comment.[11] We think that this obvious similarity to UGe_2 may provide the second example of the coexistence of the superconductivity with a strong ferromagnetism when the pressure study for UCu_2Si_2 is performed.

Next, in order to determine the magnetic part $\rho_m(T)$, we have used the classical method to separate the phonon contribution $\rho_{ph}(T)$ from the measured resistivity of UCu_2Si_2 by taking into account the electrical resistivity of the nonmagnetic isostructural $ThCu_2Si_2$. Thus, in the inset of Fig. 5 we display its temperature dependence of the resistivity, $\rho(T) = \rho_o + \rho_{ph}(T)$, which behaves as a typically metallic material, having rather a low value of the residual resistivity ρ_o (2.44 $\mu\Omega$·cm). The obtained data were then fitted to the generalized Bloch-Grüneissen (BG) relation, $\rho_{BG}(T)$,[40] given by Eq. (3) [red (dark gray) solid line in the inset]:

$$\rho_{BG}(T) = \rho_0 + 4R\left(T/\Theta_D^R\right)^n \int_0^{\Theta/T} \frac{z^n dz}{(e^z - 1)(1 - e^{-z})}. \quad (3)$$

The term ρ_{BG} was calculated with $n = 5$. R reflects the strengths of the electron-phonon interaction, and its value is 0.13 $\mu\Omega$·cm·K^{-1} and the Debye temperature $\Theta_D^R = 297(2)$ K. As seen, we did not need to include into Eq. (3) the additional Mott interband scattering s-d term, $-\mathrm{KT}^3$, because a good overall fit with a BG law is observed up to RT. All these terms yield the similar T variation, as found for many other nonmagnetic intermetallic reference compounds used as a phonon contribution, e.g., for YCu_2Si_2,[11] where $R = 0.129$ $\mu\Omega$·cm·K^{-1} and $\Theta_D^R = 296$ K.

In Fig. 5 we show on the semilogarithmic scale the two corresponding $(\rho - \rho_0)(T)$ curves for the following cases:

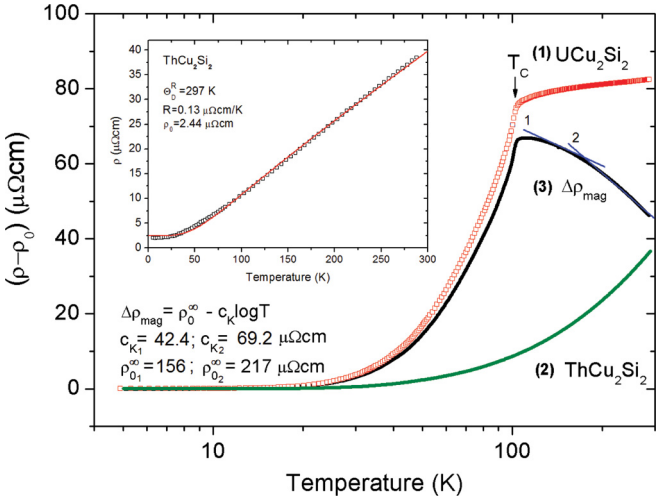

FIG. 5. (Color online) The differences $(\rho - \rho_0)$ of (1): UCu_2Si_2 (along the c axis) and (2): $ThCu_2Si_2$, as well as the difference of (3): $\Delta\rho_{mag} = (\rho - \rho_0)_{(1)} - (\rho - \rho_0)_{(2)}$, all as a function of $\log(T)$. The solid lines 1 and 2 represent Eq. (4) for different parameters presented in the figure. The inset displays the fitting of the experimental $\rho(T)$ data of $ThCu_2Si_2$ to Eq. (3).

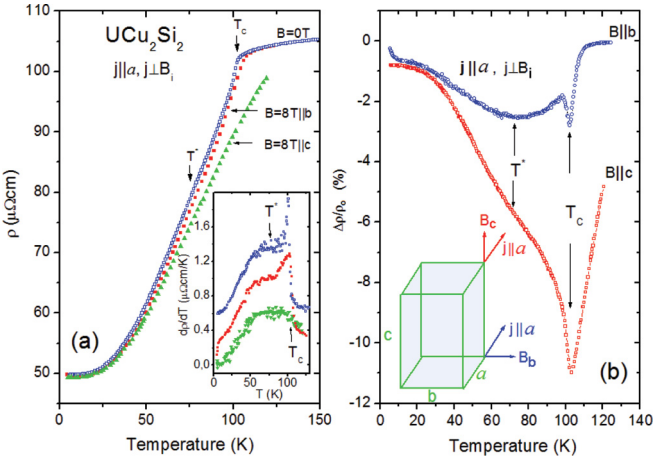

FIG. 6. (Color online) (a) Electrical resistivity as a function of temperature measured at applied magnetic fields of 0 and 8 T. For the latter case the magnetic field was directed along the b and c axes, as presented in the inset of (b). In the same figure the $\Delta\rho/\rho_0(T)$ functions are given for **B** applied along the two above directions.

(1) UCu_2Si_2 (measured along the c axis) and (2) $ThCu_2Si_2$ (measured on the polycrystalline sample), where ρ_o is the residual resistivity due to lattice defects and impurities as well as to electron scattering on the narrow domain walls in the case of the U-based compound. In turn, curve (3) represents the difference $\Delta\rho_{mag}$ between curves (1) and (2). The previous difference presents clearly a $\log(T)$ behavior at higher temperatures, characteristic of the single-Kondo effect. Previously, Hiebl[11] was the first author to consider such a dependence for his polycrystalline solid solutions $U_{1-x}Y_xCu_2Si_2$ (where $x = 0$, 0.5, and 0.875). We, following Ref. 11, have analyzed our results within the theory of Cornut and Coqblin,[41] who describe both the influence of the Kondo effect and the CEF interactions on the electrical properties of some Ce-based intermetallic compounds. As a result of a combined effect of the Kondo and CEF interactions, we also display in Fig. 5 the magnetic contributions $-\log(T)$ to the total resistivity in the paramagnetic state as the possible two lines with different slopes C_{Ki} using the standard formula:

$$\Delta\rho_{mag}(T) = \rho_{0i}^{\infty} - C_{Ki}\log(T), \qquad (4)$$

where $\rho_{0i}{}^{\infty}$ is the temperature-independent spin-disorder term and C_{Ki} is the Kondo coefficient. The corresponding parameters are given in Fig. 5. The change in the slope of $\Delta\rho_{mag}$ (T) at about 180 K is attributed to the CEF split energy levels. Hence, in a similar way to the latter theory, we have tried to find from the ratio of the respective Kondo coefficients C_{K1}:$C_{K2} = 5/8$ the degeneracies of the low-lying crystal-field split levels. In our present case we can consider only those levels being close to the ground state, and analogous results have been earlier obtained in Refs. 11 or 42. The results concerning the CEF effect are relatively ambiguous, because the two temperature ranges marked in our Fig. 5 as parts 1 and 2 are rather too small. Nevertheless, a similar magnitude in the ratio of the respective Kondo coefficients in our and Hiebl's works may, however, suggest the presence of the four lowest lying, close in energy, levels and one more distant singlet. These results in some degree may support the conclusion that, in the case of UCu_2Si_2, we have to do with the U^{4+} ion with the nearly localized $5f^2$ configuration.

The compound UCu_2Si_2 presents both an FM order with a relatively large Curie temperature of about 100–108 K, depending on a used sample, and the UKL behavior characteristic of the Kondo-lattice effect in actinide systems.[16,20] This new scenario presented here for UCu_2Si_2 enlarges the list of the growing family of the UKL FM compounds, with some already known uranium compounds such as UTe[43] or recently studied neptunium compounds like $NpNiSi_2$[44] or Np_2PdGa_3.[45] This peculiar UKL behavior arises from the localized spins of the actinide atoms, which are larger than the $s = 1/2$ conduction electron spins and, consequently, cannot be completely screened at very low temperatures.

In Fig. 6(a) we show the temperature-dependent resistivity of UCu_2Si_2 taken at $B = 0$ and 8 T only for the case $\mathbf{j}\|a$ due to the flat shape of the measured sample for which the c axis is perpendicular to its flat surface. The magnetic field B was applied perpendicular to the direction of the current. There are, however, two such directions, i.e., along either the b or c axis [see Fig. 6(b)]. In both cases the overall resistivity measured up to 120 K under the magnetic field is lower than that at $B = 0$. The considerably larger effect, however, occurs for $B = 8$ T$\|c$. In the inset to this figure, we display also the temperature derivatives, $d\rho(T)/dT$, of these three $\rho(T)_i$ curves. As seen, the sharp peak at T_C at $B = 0$ becomes, at a field of 8 T, lower and wider for $\mathbf{B}\|b$ and completely disappears where $\mathbf{B}\|c$, while the shape of all the humps at T^* becomes for all these three curves practically unchanged. This fact may indicate that the previous humps are not practically sensitive to an applied magnetic field, at least up to 8 T. In turn, in Fig. 6(b) we have plotted the MR, $\Delta\rho/\rho_0$, defined as $\Delta\rho/\rho_0 = [\rho(B) - \rho(0)]/\rho(0)$, as a function of temperature for the two configurations where $\mathbf{B}_b$ or $\mathbf{B}_c$ are applied perpendicularly to $\mathbf{j}\|a$, as shown in the inset of this

figure and described previously. As illustrated, the measured transverse MR of UCu_2Si_2 in the temperature range of the FM order has an expected negative sign. However, the temperature dependence of MR is quite unusual. The $\Delta\rho/\rho_0(T)$ functions found at $B = 8$ T first go through a diffuse negative hump at $T_{\min} \approx 76$ K, i.e., about 3/4 T_C, as it was also the case of the resistivity derivatives considered previously. By this analogy we denote that $T_{\min} \equiv T^*$. As we have argued below, just the presence of magnetic fluctuations in the FM order can produce a fairly large negative MR. Then, with increasing temperature the MR shows a sharp negative minimum at $T_C = 103$ K, considerably larger along the c than a axis. These indicate a large critical scattering of electrons at T_C, characteristic of the second-order type transitions. A very rapid change of this dependence, as T is increased above T_C, gives no evidence of another critical electron anomaly, signalized in our sample at an approximated T_N being very close to T_C, as presented in Fig. 3 by the $\chi_{ac}(T)$ and $dM(T)/dT$ dependencies. This fact is also supported by our specific heat measurements,[36] where we have found only one fairly small transition maximum at T_C in contrast to the two such maxima appearing at T_C and T_N, as reported in Refs. 12 and 13.

Having in mind the above diffuse anomalies around T^* in the transverse MR, one can see a similarity with such anomalies previously observed in the transverse MR of UGe_2,[39,46] pointing to the presence of strong magnetic fluctuations reaching its intensity maximum of about 40%, deeply below T_C, i.e., at $T^* \approx 1/2T_C$. Thus, the above similarity and the discussion about the FS (see below) may provide another example of the superconductivity coexisting with the strong FM order under applying pressure, owing to a depression of these magnetic fluctuations being of a probable C-SDW origin. Thus, fluctuations of this type existing in the whole FM order manifest themselves in the form of bulges or humps described above (see also the discussion by Watanabe and Miyake[47] describing such fluctuations in UGe_2).

The transverse MR data obtained in applied magnetic fields up to 8 T and taken at several temperatures [indicated in Figs. 7(a) and 7(b)] for the current $\mathbf{j}\|a$ and the magnetic fields either along b or c, $\mathbf{B}_b$ or $\mathbf{B}_c$, behave in quite a different way. As $\Delta\rho/\rho_0$ is measured for $\mathbf{B}\|b$ [Fig. 7(a)], one observes first its negligible change in low fields, and then in higher field strengths its negative values grow more rapidly up to about 4 T. Above this value, $\Delta\rho/\rho_0$ measured at 20 K goes through a minimum, while the MR curves taken at 40 and 60 K go through wide knees. Above these features, they either slowly decrease almost linearly in higher fields, as that measured at 20 K, or less or more increase as those at 40 and 60 K, respectively, showing a tendency to saturation.

During the reverse field period, i.e., as the strength of the magnetic field decreases, a large hysteresis in $\Delta\rho/\rho_0(B)$ takes place in the region of low fields below 4 T. It appears that for all above three temperatures, the remaining MR, $\Delta\rho/\rho_0(0)$, becomes large, and for these three cases it amounts to about -0.75%. On the other hand, when $\Delta\rho/\rho_0$ is measured along $\mathbf{B}\|c$ [Fig. 7(b)], one observes first its strong drop to values of -1.5% at 4.2 K and to -2.2% at 60 K in a field period up to 0.5 and 0.2 T, respectively (see the inset to this figure). The measured curves of transverse MR above these limited

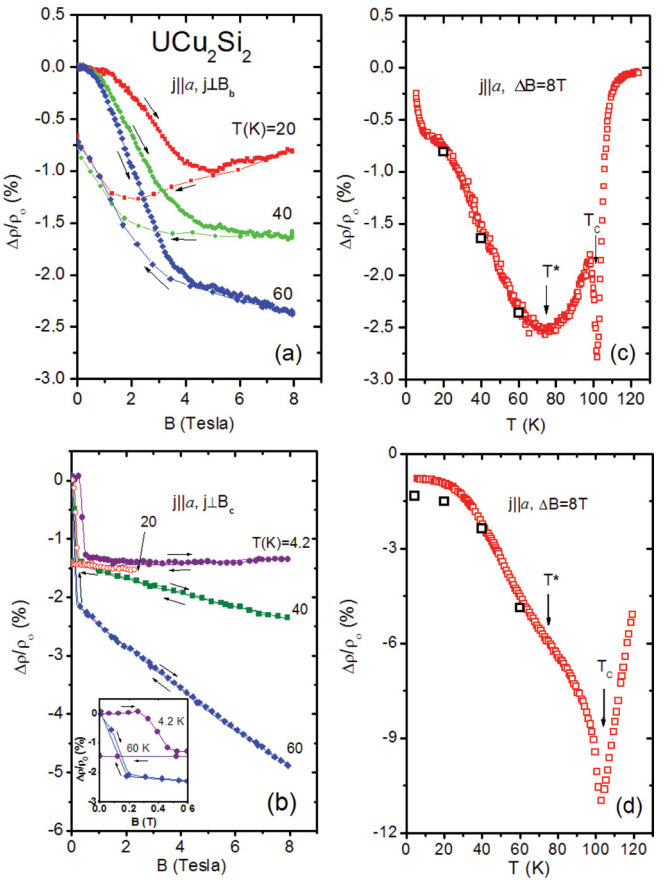

FIG. 7. (Color online) (a) and (b) Field dependencies of MR measured at several temperatures indicated in the figures for the two cases, i.e., as $\mathbf{j}\|a$, then the magnetic field is applied along either b or c axes, respectively. The inset in (b) shows on enlarged scale the hysteresis of MR at 4.2 and 60 K in low magnetic field strengths. (c) and (d) Temperature dependencies of MR with $\mathbf{j}\|a$ at constant applied magnetic field of 8 T for the previous two field directions, respectively. The black open squares seen in (c) and (d) are plotted to verify the values obtained at 8 T in the field dependencies of MR.

fields start to vary further with increasing fields almost as straight lines having, however, different slopes. As shown in Fig. 7(b), no sign of any hysteresis is apparent in the previous MR variation. It is, however, difficult to make at this step of measurements any interpretation of the above clear differences in the $\Delta\rho/\rho_0(B)$ variations arising with an application of the magnetic field in the two possible directions that are perpendicular to the current directions. In turn, Figs. 7(c) and 7(d) show that the $\Delta\rho/\rho_0(T)$ curves of UCu_2Si_2 measured at 8 T can be partly reproduced by the 8 T data found in the $\Delta\rho/\rho_0(B)$ dependencies. Some small deviation of the two square points seen at low temperatures when $\mathbf{B}\|c$ is caused by hysteretic behavior of MR only in these regions of temperature.

D. Thermoelectric power

The temperature-dependent TEP, S_i, of UCu_2Si_2 taken for a gradient ΔT along $i = a$ and c axes is shown in Fig. 8. As this figure indicates, the TEP also shows anisotropic behavior. Nevertheless, both $S_a(T)$ and $S_c(T)$ exhibit negative shallow minima at $T_{\min} = 25$ and 30 K with magnitudes of -2.5 and

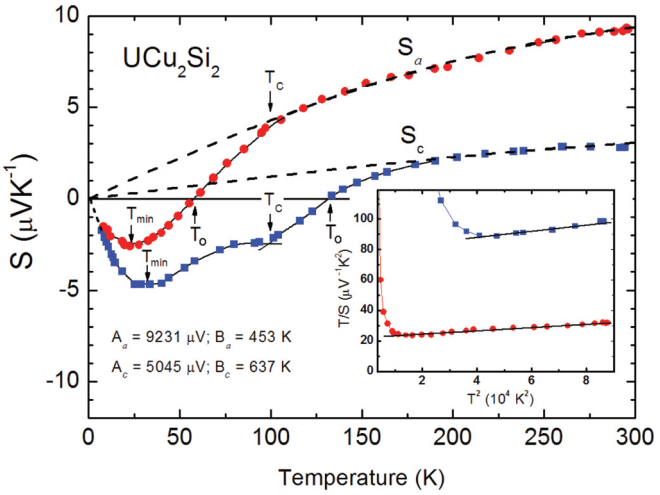

FIG. 8. (Color online) Temperature dependencies of the thermoelectric power S_i of UCu_2Si_2 for different directions $i = a$ and c. The inset shows T/S_i vs T^2. The fittings denoted by dashed lines were made using Eq. (5).

-4.9 V/K followed by a change in sign into a positive one at $T_0 = 60$ and 170 K, respectively.

The TEP of anomalous cerium and uranium compounds is generally large and can present a peak due to the CEF at temperatures corresponding to a fraction (1/3 to 1/6) of the total CEF splitting (Δ_{CF})[48] or also another peak corresponding to the Kondo temperature T_K.[49,50] The situation is often complicated, because there are a number of contributions with different origins, mainly the phonon and magnon ones.

However, the TEP of the UCu_2Si_2 compound shown in Fig. 8 is relatively small and presents with a high probability a Kondo-FM-CEF behavior; the TEP of such a more complicated case has not yet been discussed theoretically. There is a shallow minimum in our single-crystal data at 25 or 30 K for the a and c directions, and this negative peak could correspond to a small fraction of the CEF splitting roughly equal to about 0.3 Δ_{CF} within the Kondo-CEF model of Ref. 48. We can also consider the temperature T_{min} as being connected exclusively to the Kondo effect, which is just predicted to give a fairly wide peak close to T_K.[49,50]

Any pronounced feature at T_C is only apparent in $S_c(T)$ in the form of a shoulder where a distinct change in the slope of this function takes place, as shown in Fig. 8. Thus, it indicates that the electron transport perpendicular to the c axis is rather less sensitive to the magnetic phase transition. This seems to be adequate because of the fact that the FM order in UCu_2Si_2 is just along the c axis.[8] Especially, we can mention here a similar behavior of the Kondo-FM system CePt.[51] A large similarity in $S(T)$ along the a and c directions to that in our compound exists also for $UCoGa_5$.[52] Thus, the interpretation of the TEP behavior in the FM domain below T_C is not very clear up to now. Here, we must mention that there also exists another explanation. According to the semiphenomenological model developed by Fisher,[53] who has discussed the Seebeck coefficient behavior of several Ce compounds in the frame of the Anderson Hamiltonian, the total thermopower, $S_{total}(T)$, consists of two contributions $S^{(1)}$ and $S^{(2)}$. They have opposite signs and were called the "Kondo" and "resonance" terms, respectively. The latter emerges owing to spin interactions. Due to the opposite signs of these two terms, their superpositions lead to a lowering of the overall positive magnitudes of the $S_{total}(T)$ function and owe to the change of the sign at T_0, thus forming a negative broad minimum.

On the other hand, the high T domain of temperature, when the TEP becomes positive, can be interpreted by a phenomenological model introduced by Gottwick *et al.*[54] At high T, a strong f-conduction electron hybridization still remains, and the model is based on the two-band conductor model, where the conduction electrons are assumed to be scattered by a $5f$ quasiparticle band of a Lorentzian form. The TEP is then given by

$$S(T) = \frac{AT}{B^2 + T^2}, \quad A = \frac{2\Delta}{|e|}, \quad B^2 = 3\frac{\Delta^2 + \Gamma^2}{\pi^2 k_B^2}, \qquad (5)$$

where Δ is the distance between the Lorentzian peak energy and the Fermi level (E_F), and Γ is the width of the Lorentzian due to the f-conduction electron hybridization. We find the values of the constants A_i and B_i, given in Fig. 8, by fitting the curves from the previous plot of T/S against T^2, and the other parameters are calculated: $\Delta_\alpha = 4.62$ and $\Delta_c = 2.52$ meV, $\Gamma_a = 70.7$ and $\Gamma_c = 99.5$ meV.

At RT, the TEP magnitudes are rather low and amount to 2.6 for S_c and 9 μV/K for S_a, as one can predict from the Fisher theory. In the region of temperatures above T_0, where $S_i(T)$ has for both directions a positive curvature, the T/S_i vs T^2 dependencies (shown in the inset of this figure) behave linearly above about 100 K for $S_a(T)$ and 200 K for $S_c(T)$. Therefore, in the paramagnetic region the overall positive run of the TEP in UCu_2Si_2 is reminiscent of that in the Ce-based Kondo lattices, characterized by a broad growing of the positive TEP up to 100 K due to the interplay of the Kondo and CEF-combined interactions. The curve giving T/S_i vs T^2 straight lines by Eq. (5) is working in several cerium compounds.[55] It is interesting to note that the downward deviation of the experimental points from the theoretical curve $S_a(T)$ just starts at T_C. Finally, we have obtained good fits of the TEP at sufficiently high temperature, while the situation is not so clear at low temperature below T_C and requires further studies of S_i (T) function in magnetic field.

E. The Fermi surface

The whole FS of UCu_2Si_2 in its FM state with the magnetic moments arranged along the c axis is presented in Fig. 9. It has been calculated based on the fully relativistic band structure results, reported in Ref. 22, obtained by the full-potential local-orbital (FPLO) code in the local spin-density approximation with orbital-polarization correction (LSDA + OP) (see Ref. 22 and references therein). The respective densities of states, as inferred from the previous approach, were already plotted in Fig. 2(a) of Ref. 22, while the value of 1.9 μ_B for the total FM moment of the U atom was given in Table II therein.

As Fig. 9 indicates, the computed FS of UCu_2Si_2 exists in three nondegenerate bands, numbered as 91–93, drawn separately in the tetragonal Brillouin zone (BZ) boundaries of the $ThCr_2Si_2$-structure type. The overall shapes and characters

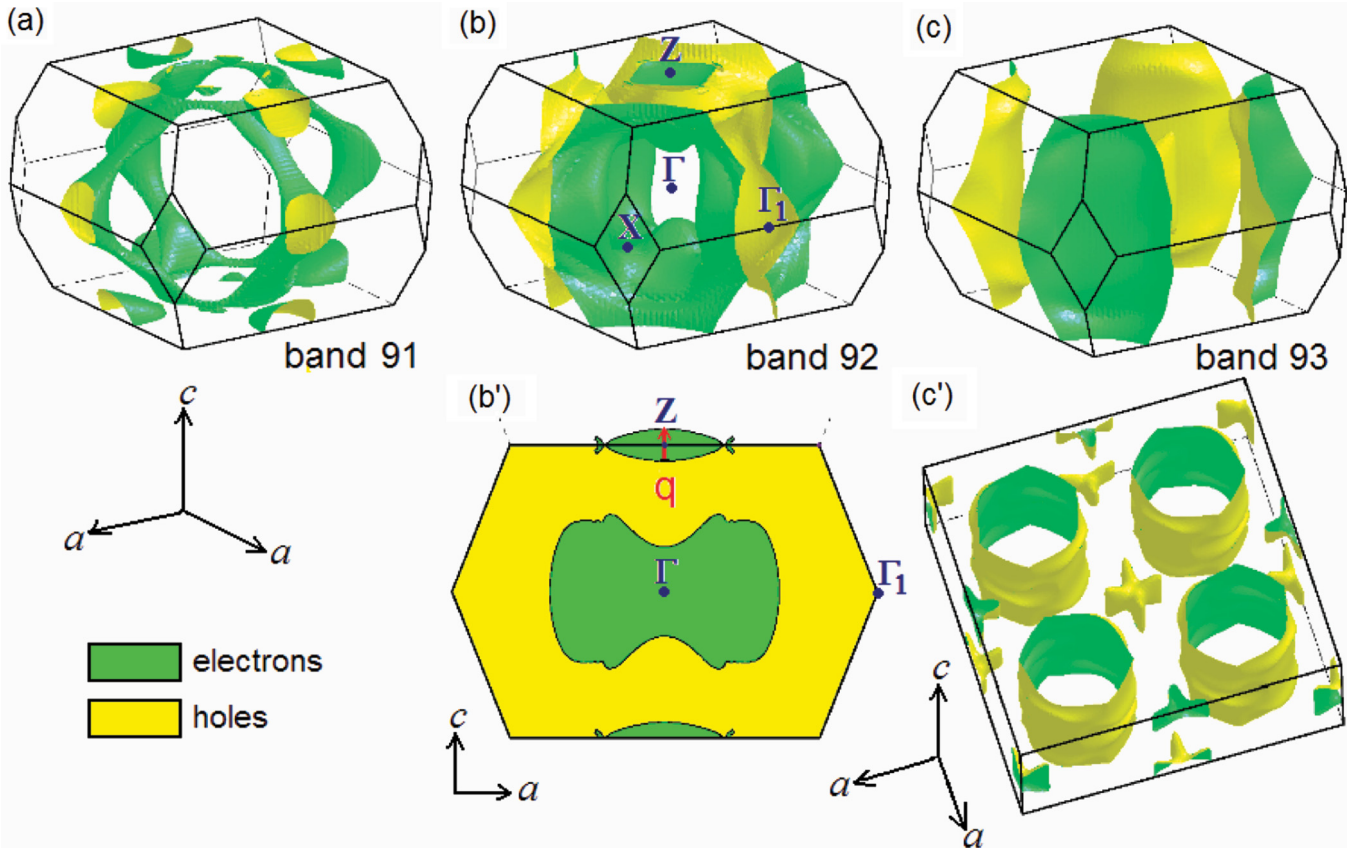

FIG. 9. (Color online) The FS of UCu_2Si_2 in the FM ordered state (along the c axis), which exists in three conduction bands, numbered as (a) 91, (b) 92, and (c) 93, computed employing the LSDA + OP approach, drawn in the tetragonal BZ of the $ThCr_2Si_2$ type. (b′) The ac plane section of the FS sheet from the 92th band, displayed in (b), where the red (dark gray) arrow denotes the nesting vector $\boldsymbol{q} = [0, 0, 0.116]$ for the spanning surfaces of the electron pillow, being centered at the Z point of BZ. In turn, (c′) visualizes the same FS sheet as in (c) but is drawn in the conventional tetragonal unit cell boundaries. Green (dark) and yellow (light) colors correspond to electrons and holes, respectively.

of the presented FS sheets are similar to those obtained previously for the same compound[23] but using the different RSPLAPW band structure method.[24] The latter results are shown in Fig. 3(c) of Ref. 23, being the same as ours but having different numbers, because they are otherwise counted by starting from higher valence bands. The FS sheet coming from the lowest 91th band, displayed in Fig. 9(a) and corresponding to the "band 41-hole" in Fig. 3(c) of Ref. 23, is rather three-dimensional (3D) and consists mainly of interconnected hole pipes. In comparison, such pipes are also shown in Ref. 23, but they look rather as being disconnected. The FS sheet presented in Fig. 9(b), originating from the 92th band, possesses also a 3D character and contains mainly corrugated holelike pillars. They closely resemble those drawn in Fig. 3(c) of Ref. 23, occurring in the "band 42-hole." However, a poor resolution of that figure disables us from making any comparison of their details. It is most worthwhile to note here that there is also a small, flat electron pillow, centered at the Z point. Such a similar FS element, but rotated by 45° with respect to our finding, is visible also in Fig. 3(c) of Ref. 23. Interestingly, the authors of that paper have associated this element with de Haas-van Alphen (dHvA) orbits, called δ and δ'. Unfortunately, in the performed dHvA experiment, reported in Ref. 23, solely the smaller orbit, δ, has been found. To give a better look at this piece of FS, we present in Fig. 9(b)′ the ac-plane section of our FS sheet to show that the electron pillow has almost perfect nesting properties along the c axis. It is worth underlining here that the nesting vector $\boldsymbol{q} = [0, 0, 0.116]$ inferred by us (marked by red/dark gray arrow in this figure) and the magnetic propagation vector $\mathbf{k_z}$ of the incommensurate SDW phase, found in Ref. 8, have the identical magnitudes and directions. Hence, there exists a possibility of appearing (e.g., under pressure) superconductivity in the FM UCu_2Si_2, such as that realized earlier in the case of UGe_2 (for literature see, e.g., Ref. 46). This phenomenon is most likely expected to be mediated by the magnetic fluctuations. Interestingly, the FS sheet, originating from the highest 93th band, displayed in Fig. 9 in the BZ (c) as well as in boundaries of the conventional u.c. (c'), is constructed from quasi-2D electron cylinders, centered at the X points of the BZ corners, with their axes arranged parallel to the c axis. In addition, a small electron crosslike element occurs at the Γ point, which is clearly visible in Fig. 9(c)′. Both types of FS elements are also present in the "band 43-electron" FS sheet drawn in Fig. 3(c) of Ref. 23. In comparison, our cylinders seem to be less corrugated. Thus, we take into consideration the speculation that they might be also responsible for appearing p-wave superconductivity in UCu_2Si_2, in a similar way as in UGe_2,[46,56] provided that the C-SDW fluctuations would be suppressed by applying pressure, i.e., $T^* \approx 0$.

IV. CONCLUSIONS

We have studied a single-crystalline sample of UCu_2Si_2 obtained by the Cu-flux synthesis. Our sample, in the temperature dependencies of both ac-susceptibility and low-field magnetization measurements, shows only very weak signals of the presence of the IL-SDW phase, which was so clearly presented in the neutron-diffraction experiment made by Honda *et al*.[8] The detailed studies of our sample by magnetization, electrical resistivity, but especially by MR and thermoelectrical power, do not show the presence of the IL-SDW phase. This finding is in full agreement also with our heat capacity measurements.[36] Such a notably dissimilar magnetic behavior of our sample to other reports seems to be a common feature also to other tetragonal UT_2Si_2 ternaries, where the effect of strong sample dependence takes place (see, for example, Ref. 57).

Using a nonmagnetic isostructural reference compound, $ThCu_2Si_2$, we were able to point out clearly that the U-based silicide is really a Kondo-like ferromagnet. Thus, for such actinide compounds the special UKL theory has been presented in the literature.[16,20] The electrical resistivity at low temperatures does not show T^2 dependencies along two main crystallographic directions, but it is rather dominated by a gapped spin-wave model. However, the most interesting feature in the transport properties of UCu_2Si_2, made outside of and in magnetic fields up to 8 T, is the presence of magnetic fluctuations with the characteristic temperature $T^* < T_C = 103$ K, coexisting with the strong magnetic order. This fully resembles the behavior of UGe_2.[39,47] It may be a signature that also UCu_2Si_2 may under pressure become a superconductor despite the presence of the strong FM ordering.

Finally, taking into account the previous findings, we can conclude that our data as well as those reported earlier indicate the dualism of the $5f$ electrons in the present study of UCu_2Si_2 being a strongly anisotropic ferromagnet and exhibiting the Kondo effect. In this picture the FM order comes from the part of the U $5f$ highly localized electrons giving rise to the high T_C value. Hence, due to the existing huge inner magnetic field caused by this local FM arrangement below T_C, the SDW phase occurs in a form of magnetic fluctuations only. A situation, however, may be diametrically changed after diminishing this inner field to a small value near T_C. Then, the SDW phase emerges up to its T_N if for a given sample $T_N > T_C$. In our situation, $T_N \approx T_C$, thus, we practically do not detect this phase. This is quite a new insight into the magnetic phase transitions in some of the uranium systems, especially occurring among tetragonal 1:2:2 phases. Therefore, one cannot expect to detect any SDW phase in the presence of the local FM order, as such a test, carried out in the case of UGe_2 using neutron diffraction experiment, has pointed out.[58]

ACKNOWLEDGMENTS

We express our thanks to A. Zaleski for making available the ac-susceptibility data. We are grateful to R. Gorzelniak and D. Badurski for the technical assistance. We are also in debt to C. Sułkowski for the TEP measurements and Z. Bukowski for growing the single crystal. We also thank A. Szajek for making available the FPLO results presented in Ref. 22. The Computing Center at the Institute of Low Temperature and Structure Research PAS in Wrocław is also acknowledged for the use of the supercomputers and technical support.

*Corresponding author: r.troc@int.pan.wroc.pl

[1] L. Chełmicki, J. Leciejewicz, and A. Zygmunt, J. Phys. Chem. Solids **46**, 529 (1985).
[2] Z. Ban and M. Sicirica, Z. Anorg. Allg. Chem. **356**, 96 (1967).
[3] J. Leciejewicz and A. Szytuła, Acta Phys. Pol. A **72**, 65 (1982); J. Magn. Magn. Mater. **63–64**, 190 (1987).
[4] J. A. Mydosh and P. M. Oppeneer, Rev. Mod. Phys. **83**, 1301 (2011).
[5] P. S. Riseborough, B. Coqblin, and S. G. Magalhães, Phys. Rev. B **85**, 165116 (2012), see also Ref. 20.
[6] A. Szytuła, S. Siek, J. Leciejewicz, A. Zygmunt, and Z. Ban, J. Phys. Chem. Solids **49**, 1113 (1988).
[7] A. L. Giorgi, A. C. Lawson, A. Goldstone, K. J. Volin, and J. D. Jorgensen, J. Appl. Phys. **63**, 3604 (1988).
[8] F. Honda, N. Metoki, T. M. Matsuda, Y. Haga, and Y. Ōnuki, J. Phys.: Condens. Matter **18**, 479 (2006).
[9] K. Hiebl, P. Rogl, C. Horvath, K. Remschinig, and H. Noël, J. Appl. Phys. **67**, 943 (1990).
[10] M. S. Torikachvili, R. F. Jardim, C. C. Becerra, C. H. Westphal, A. Paduan-Filho, V. M. Lopez, and L. Rebelsky, J. Magn. Magn. Mater. **104–107**, 69 (1992).
[11] K. Hiebl, J. Phys. Soc. Jpn. **67**, 2048 (1998).
[12] Z. Fisk, N. O. Moreno, and J. D. Thomson, J. Phys.: Cond. Matter **15**, S1917 (2003).
[13] T. D. Matsuda, Y. Haga, S. Ikeda, A. Galatanu, E. Yamamoto, H. Shishido, M. Yamada, J. Yamaura, M. Hedo, Y. Uwatoko, T. Matsumoto, T. Tada, S. Noguchi, T. Sugimoto, K. Kuwahara, K. Iwasa, M. Kohgi, R. Settai, and Y. Onuki, J. Phys. Soc. Jpn. **74**, 1552 (2005).
[14] R. Troć and Z. Bukowski, Phys. Status Solidi B **243**, 290 (2006).
[15] G. Zwicknagl, A. N. Yaresko, and P. Fulde, Phys. Rev. B **65**, 081103 (2002).
[16] N. B. Perkins, M. D. Núñez-Regueiro, B. Coqblin, and J. R. Iglesias, Phys. Rev. B **76**, 125101 (2007).
[17] L. M. Sandratskii and J. Kubler, Phys. Rev. B **50**, 9258 (1994).
[18] A. Mavromaras, L. Sandratskii, and J. Kübler, Solid State Commun. **106**, 115 (1998).
[19] T. Endstra, G. J. Nieuwenhuys, and J. A. Mydosh, Phys. Rev. B **48**, 9595 (1993).
[20] C. Thomas, A. S. da Rosa Simões, J. R. Iglesias, C. Lacroix, N. B. Perkins, and B. Coqblin, Phys. Rev. B **83**, 014415 (2011); see also B. Coqblin, J. R. Iglesias, N. B. Perkins, A. S. da Rosa Simões, and C. Thomas, Physica B **404**, 2961 (2009).
[21] R. Troć, M. Samsel-Czekała, and B. Coqblin, Acta Phys. Polon. A **121**, 1023 (2012).
[22] J. A. Morkowski, G. Chełkowska, M. Werwiński, A. Szajek, R. Troć, and C. Neise, J. Alloys Compd. **509**, 6994 (2011), and references therein.

[23]T. D. Matsuda, S. Ikeda, E. Yamamoto, Y. Haga, H. Shishido, H. Yamagami, R. Settai, and Y. Ōnuki, J. Phys. Soc. Jpn. **79**, 114712 (2010).
[24]H. Yamagami, J. Phys. Soc. Jpn. **67**, 3176 (1998).
[25]G. Sheldrick, *SHELXS-97, and SHELXL-97, Programs for Crystal Structure Refinement* (University of Göttingen Press, Göttingen, Germany, 1997).
[26]Z. Ban and M. Sikirica, Acta Cryst. **18**, 594 (1965).
[27]J. Leciejewicz, S. Siek, and A. Szytuła, J. Less-Comm. Met. **144**, L9 (1988).
[28]J. S. Kim, C. S. Jee, W. W. Kim, B. Andraka, P. Kumar, and G. R. Stewart, Phys. Rev. B **44**, 7473 (1991); K. Hiebl and P. Rogl, J. Nucl. Mater. **144**, 193 (1987).
[29]M. Kuznietz, H. Pinto, and M. Melamud, Phys. Rev. B **51**, 16410 (1995).
[30]M. Kuznietz, J. Phys.: Cond. Matter. **15**, 8957 (2003).
[31]S. F. Matar, V. Siruguri, and V. Eyert, J. Magn. Magn. Mater. **305**, 264 (2006).
[32]H. Takahashi and T. Kasuya, J. Phys. C **18**, 2697 (1985).
[33]Z. Żołnierek and J. Mulak, J. Magn. Magn. Mater. **140–144**, 1393 (1995).
[34]M. W. McElfresh, L. Rebelsky, M. S. Torikachvili, H. Borges, K. Reilly, S. Horn, and M. B. Maple, J. Appl. Phys. **67**, 5218 (1990).
[35]S. B. Roy, A. K. Pradhan, P. Chaddah, and B. R. Coles, Solid State Commun. **99**, 563 (1996).
[36]R. Troć, A. Pikul, E. Colineau, and H. Misiorek (to be published).
[37]T. Homma, H. Amitsuka, T. Sakakibara, K. Sugiyama, and M. Date, Physica B **186–188**, 684 (1993).
[38]N. H. Andersen and H. Smith, Phys. Rev. B **19**, 384 (1979).
[39]R. Troć, J. Magnetics (Korea) **9**, 89 (2004), and references therein.
[40]G. Grimvall, *The Electron-Phonon–Interactions in Metal* (North-Holland, Amsterdam, 1981).
[41]D. Cornut and B. Coqblin, Phys. Rev. B **5**, 4541 (1972).
[42]D. Kaczorowski, P. Rogl, and K. Hiebl, Phys. Rev. B **54**, 9891 (1996).
[43]J. Schoenes, J. Less-Comm. Met. **121**, 87 (1986).
[44]E. Colineau, F. Wastin, J. P. Sanchez, and J. Rebizant, J. Phys.: Condens. Matter **20**, 075207 (2008).
[45]V. H. Tran, J.-C. Griveau, R. Eloirdi, W. Miiller, and E. Colineau, Phys. Rev. B **82**, 094407 (2010).
[46]R. Troć, Acta Phys. Polon. B **34**, 407 (2003), and references therein; see also J. Alloys Comp. **423**, 21 (2006).
[47]S. Watanabe and K. Miyake, J. Phys. Soc. Jpn. **71**, 2489 (2002).
[48]A. K. Bhattacharjee and B. Coqblin, Phys. Rev. B **13**, 3441 (1976).
[49]R. M. Konik, Phys. Rev. B **68**, 104435 (2003).
[50]B. Coqblin, B. Chevalier, and V. Zlatič, in NATO Program on *Properties and Applications of Thermoelectric Materials* (Springer, Dordrecht, Netherlands, 2009).
[51]J. Sakurai, A. Iwasaki, Q. Lu, D. Huo, Y. Isikawa, J. Rodriguez Fernandes, and J. Gomez Sal, J. Phys. Soc. Jpn. **71**, 2829 (2002).
[52]R. Troć, Z. Bukowski, C. Sułkowski, H. Misiorek, J. A. Morkowski, A. Szajek, and G. Chełkowska, Phys. Rev. B **70**, 184443 (2004).
[53]K. H. Fischer, Z. Phys. B **76**, 315 (1989).
[54]U. Gottwick, K. Gloos, S. Horn, F. Steglich, and N. Grewe, J. Magn. Magn. Mater. **47–48**, 536 (1985).
[55]Y. Bando, T. Suemitsu, K. Takagi, H. Tokushima, Y. Echizen, K. Katoh, K. Umeo, Y. Maeda, and T. Takabatake, J. Alloys Compd. **313**, 1 (2000).
[56]A. B. Shick and W. E. Pickett, Phys. Rev. Lett. **86**, 300 (2001).
[57]T. Plackowski, D. Kaczorowski, and J. Sznajd, Phys. Rev. B **83**, 174443 (2011).
[58]A. Huxley, I. Sheikin, E. Ressouche, N. Kernavanois, D. Braithwaite, R. Calemczuk, and J. Flouquet, Phys. Rev. B **63**, 144519 (2001).